A Novel Array Error Estimation Method for Azimuth Multichannel SAR

Xile Ma[*]**, Zhen Dong, Zaoyu Sun, Feng He, and Diannong Liang**

Abstract—Minimum side-zone power to center-zone power ratio (MSCR) method is presented to estimate array errors of azimuth multichannel synthetic aperture radar (SAR). Spaceborne azimuth multichannel SAR is one of the most promising candidates for achieving high-resolution wide-swath imaging. However, array errors brought in by instrument influences and aperture position errors need to be compensated. MSCR method is designed to obtain phase error estimates by minimizing side-zone power to center-zone power ratio, where the side-zone and the center-zone indicate the intervals far from and around Doppler centroid respectively. The proposed method achieves significantly improved performance on phase error estimation especially when signal to noise ratio is low. Experiment results confirm the validity and solidity of the method.

1. INTRODUCTION

Spaceborne synthetic aperture radar (SAR) system [1–5] proves to be an extremely useful surveillance tool for remote sensing of the earth. Innovative techniques have been investigated to realize high-resolution wide-swath observation [6–8]. Among those techniques, azimuth multichannel SAR concept [9–13] proves to be one of the most promising candidates. By splitting the conventional long receive antenna in azimuth direction into multiple subapertures with independent receive channels, additional samples are received for each transmitted pulse. This allows for an improved azimuth resolution with a very low pulse repetition frequency (PRF), thereby maintaining the swath width Another implementation of azimuth multichannel SAR that has been proposed is a constellation of formation-flying satellites [11]. Considering disadvantages of this implementation at present stage [10], in this paper, we focus on single-platform systems.

A series of algorithms have been discussed to reconstruct ambiguous spectrum [9–11]. Array errors brought in by instrument influences and aperture position errors are inevitable. They degrade the performance of the reconstruction and have to be compensated. For single-platform azimuth multichannel SAR systems, the errors are mainly identified to phase errors [11–13], given that the gain imbalance can be removed by amplitude equalization. Orthogonal subspace method (OSM) is investigated in [11] for array error calibration. Signal subspace comparison method (SSCM) and antenna pattern method (APM) are presented in [12] for phase error estimation. SSCM gives similar estimation performance to OSM whereas requires lighter computational load. APM is also very efficient; however, it requires an accurate knowledge of the azimuth antenna pattern. The adaptively weighted least square (AWLS) method [13] estimates the phase errors by minimizing the power outside the processed Doppler bandwidth (PDB). It achieves an improved performance especially for low signal to noise ratio (SNR).

In this paper, minimum side-zone power to center-zone power ratio (MSCR) method is presented for phase error estimation. It obtains further improved performance at the low-SNR region. Succeeding sections are organized as follows. In Section 2, principle of signal reconstruction of azimuth multichannel

SAR is reformulated. In Section 3, we present MSCR method in detail. Besides, influence of nonuniform sampling is investigated. In Section 4, experiments are performed to confirm the validity of the proposed method. Conclusions are presented in Section 5.

2. PRINCIPLE OF SIGNAL RECONSTRUCTION

2.1. Signal Model

A typical single-platform azimuth multichannel SAR system is illustrated in Figure 1, where Rx and Tx denote receive subapertures and transmit antenna respectively, v_s is sensor velocity, and Δx is along-track displacement between adjacent channels. The echoes of the mth aperture $x_m(\eta, \tau)$ evolve from their single channel counterparts $s(\eta, \tau)$ by azimuth time delay η_m and a phase shift $\xi_m = -\pi d_m^2/(2\lambda r_0)$ [9], i.e.,

$$x_m(\eta, t) = e^{j\xi_m} s(\eta + \eta_m, \tau) \cdot \sum_{k=-\infty}^{\infty} \delta(\eta - kT) \tag{1}$$

where η denotes the azimuth time, τ the fast time, λ the wavelength, r_0 the nearest slant range, $d_m = (m-1)\Delta x$, $\eta_m = (m-1)\Delta\eta$, $\Delta\eta = \Delta x/(2v_s)$, $m = \{1, 2, \ldots, M\}$, M the channel number, $T = 1/f_s$, f_s the sampling rate, i.e., PRF, and $\delta(\cdot)$ the Dirac delta function. For single-platform spaceborne systems, the quadratic phase ξ_m can be neglected [10]. To focus on phase error estimation, ξ_m is ignored in the following derivation. To make the description of azimuth signal clear, τ is omitted as well.

When phase errors and additive white noise are considered, received data is given in Range-Doppler domain as [14]

$$X_m(f_\eta) = \frac{1}{T}\left(\gamma_m \sum_{l=-\infty}^{\infty} S(f_\eta + lf_s)e^{j2\pi(f_\eta + lf_s)\eta_m} + N_m(f_\eta)\right) \tag{2}$$

where f_η denotes the Doppler frequency, and $X_m(f_\eta)$ and $S(f_\eta)$ are the Fourier transforms of $x_m(\eta)$ and $s(\eta)$, respectively. $N_m(f_\eta)$ is the noise spectrum, $\gamma_m = e^{j\varphi_m}$, and φ_m the phase error of the mth channel.

We assume that dominant spectral components are confined on interval $[f_{\eta c} - Qf_s/2, \ f_{\eta c} + Qf_s/2]$, where the positive integer Q fulfilling $B_{amb}/f_s \leq Q \leq M$ is called reconstruction coefficient, B_{amb} is Doppler bandwidth of the echoes, and $f_{\eta c}$ is Doppler centroid. Constant value T is ignored to make the expressions clear, considering that it is of no influence on signal processing and performance analysis. Then, the signal model can be expressed in matrix form as

$$\mathbf{X}(f_\eta) = \mathbf{\Gamma}\mathbf{A}(f_\eta)\mathbf{S}(f_\eta) + \mathbf{N}(f_\eta) \tag{3}$$
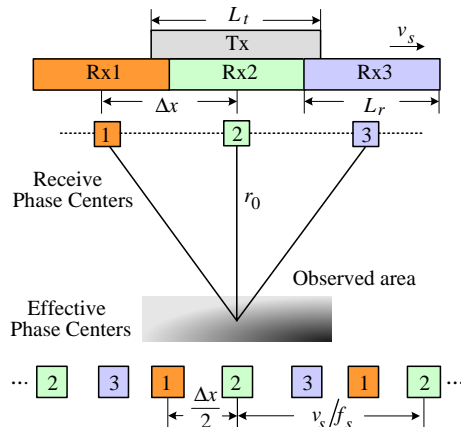
Figure 1. Spatial sampling of azimuth multichannel SAR.

where

$$\begin{cases} \mathbf{X}(f_\eta) = [X_1(f_\eta), X_2(f_\eta), ..., X_M(f_\eta)]^T \\ \mathbf{\Gamma} = \text{diag}\{\boldsymbol{\gamma}\} \\ \boldsymbol{\gamma} = [\gamma_1, \gamma_2, \ldots, \gamma_M]^T \\ \mathbf{S}(f_\eta) = [S_1(f_\eta), S_2(f_\eta), \ldots, S_Q(f_\eta)]^T \\ \mathbf{N}(f_\eta) = [N_1(f_\eta), N_2(f_\eta), \ldots, N_M(f_\eta)]^T \end{cases} \tag{4}$$

in which $[\cdot]^T$ indicates the transpose operation, $S_q(f_\eta) = S(f_\eta + l_q f_s)$ the shifted copy of $S(f_\eta)$, $l_q = q - \text{int}(\frac{Q+1}{2})$, $q \in \{1, 2, \ldots, Q\}$, $\text{int}(\cdot)$ the integer part of a real value, and $\mathbf{A}(f_\eta)$ the $M \times Q$ matrix with entries

$$[\mathbf{A}(f_\eta)]_{m,q} = e^{j2\pi(f_\eta + l_q f_s)\eta_m}; \quad 1 \le m \le M, \quad 1 \le q \le Q \tag{5}$$

where $[\cdot]_{m,q}$ denotes the matrix element located in the mth row and qth column.

The point to observe is that f_η is defined on interval $I_{Q,\text{int}((Q+1)/2)}$, where $I_{Q,q}$ is given as

$$I_{Q,q} = f_{\eta c} + \left(q - \frac{Q+1}{2}\right) f_s + \left[-\frac{f_s}{2}, \frac{f_s}{2}\right] \tag{6}$$

where $q \in \{1, 2, \ldots, Q\}$, and $\bigcup_{q=1}^{Q} I_{Q,q} = [f_{\eta c} - \frac{Q f_s}{2}, f_{\eta c} + \frac{Q f_s}{2}]$. For a finite-length discrete-time signal, we have it's spectrum via discrete Fourier transform (DFT). When an N_a-point DFT is performed on a sampled signal, the first sample of the output array represents zero frequency and the last sample represents frequency $(N_a - 1) \cdot f_s/N_a$ [14], i.e., the output array is the spectrum located on interval $[0, f_s]$. Accordingly, to obtain the spectrum on interval $I_{Q,\text{int}((Q+1)/2)}$, the direct output array need to be circularly shifted [14].

2.2. Reconstructed Doppler Spectrum

From (3), least-square (LS) estimator should be given by

$$\tilde{\mathbf{W}}(f_\eta) = \mathbf{\Gamma}\mathbf{W}(f_\eta) \tag{7}$$

where $\mathbf{W}(f_\eta) = \mathbf{A}(f_\eta)(\mathbf{A}^{\mathbf{H}}(f_\eta)\mathbf{A}(f_\eta))^{-1}$. Then we have

$$\hat{\mathbf{S}}(f_\eta) = \tilde{\mathbf{W}}^{\mathbf{H}}(f_\eta)\mathbf{X}(f_\eta) \tag{8}$$

In practice, however, $\mathbf{\Gamma}$ is unknown.

Let $\hat{\boldsymbol{\gamma}} = [\hat{\gamma}_1, \hat{\gamma}_2, \ldots, \hat{\gamma}_M]^T$ denotes an estimate of $\boldsymbol{\gamma}$, where $\hat{\gamma}_m = e^{j\hat{\varphi}_m}$ and $\hat{\varphi}_m$ denotes the estimate of φ_m. Then, the estimator used for spectrum reconstruction is actually

$$\tilde{\mathbf{W}}(f_\eta) = \hat{\mathbf{\Gamma}}\mathbf{W}(f_\eta) \tag{9}$$

where $\hat{\mathbf{\Gamma}} = \text{diag}\{\hat{\boldsymbol{\gamma}}\}$. Letting $\mathbf{w}_q(f_\eta)$ and $\tilde{\mathbf{w}}_q(f_\eta)$ be the qth column vectors of $\mathbf{W}(f_\eta)$ and $\tilde{\mathbf{W}}(f_\eta)$ respectively, we have $\tilde{\mathbf{w}}_q(f_\eta) = \hat{\mathbf{\Gamma}}\mathbf{w}_q(f_\eta)$. For any Doppler frequency $\tilde{f}_\eta \in I_{Q,q}$, we have

$$f_\eta \triangleq \tilde{f}_\eta - \left(q - \text{ceil}\left(\frac{Q+1}{2}\right)\right) f_s \in I_{Q,\text{int}((Q+1)/2)}$$

In combination with (8), we obtain the reconstructed Doppler spectrum

$$\hat{S}\left(\tilde{f}_\eta\right) = \mathbf{w}_q^{\mathbf{H}}(f_\eta)\hat{\mathbf{\Gamma}}^{\mathbf{H}}\mathbf{X}(f_\eta); \quad \tilde{f}_\eta \in I_{Q,q} \tag{10}$$

Introducing the notation $\mathbf{W}_q(f_\eta) = \text{diag}(\mathbf{w}_q(f_\eta))$, we have the power spectral density (PSD) of the reconstructed azimuth signal:

$$\left|\hat{S}(\tilde{f}_\eta)\right|^2 = \left|\hat{\boldsymbol{\gamma}}^{\mathbf{H}}\mathbf{W}_l^{\mathbf{H}}(f_\eta)\mathbf{X}(f_\eta)\right|^2 = \hat{\boldsymbol{\gamma}}^{\mathbf{H}}\mathbf{Z}\left(\tilde{f}_\eta\right)\hat{\boldsymbol{\gamma}} \tag{11}$$

where

$$\mathbf{Z}\left(\tilde{f}_\eta\right) \triangleq \mathbf{W}_q^{\mathbf{H}}(f_\eta)\mathbf{X}(f_\eta)\mathbf{X}^{\mathbf{H}}(f_\eta)\mathbf{W}_q(f_\eta); \quad \tilde{f}_\eta \in I_{Q,q} \tag{12}$$

3. MSCR METHOD

3.1. Derivation of MSCR Method

Channel errors are unknown and to be estimated. Only when $\hat{\gamma} = \gamma$, mainlobe ambiguities can be suppressed completely. Then, PSD of the reconstructed azimuth signal is approximately of the shape of the square of the round-trip azimuth antenna pattern. As illustrated in Figure 2, it attenuates with increased deviation of Doppler frequency from Doppler centroid. Though the PSD of a single azimuth line (within the same range gate) is very noisy and can not hold the attenuation property, the expected PSD $E(|\hat{S}(\tilde{f}_\eta)|^2)$ can hold the property for most ground scenes, where $E(\cdot)$ indicates the expectation value. In practice, the expected PSD is obtained by averaging a number of neighboring azimuth lines.
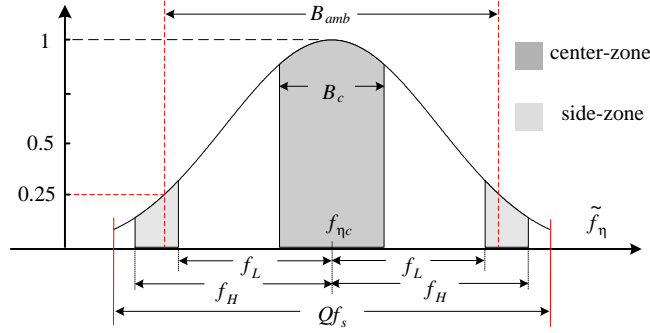
Figure 2. Illustration of the PSD of the rightly reconstructed azimuth signal (square of the round-trip azimuth antenna pattern).

Basing on the analysis presented above, we define an indicator

$$J_{\mathrm{MSCR}} \triangleq P_S/P_C \tag{13}$$

to indicate the attenuation property of the expected PSD, where $P_S \triangleq \sum\limits_{\tilde{f}_\eta \in I_S} E(|\hat{S}(\tilde{f}_\eta)|^2)$ and $P_C \triangleq \sum\limits_{\tilde{f}_\eta \in I_C} E(|\hat{S}(\tilde{f}_\eta)|^2)$ indicate the side-zone power and the center-zone power respectively, in which I_C and I_S indicate center-zone and side-zone of the estimated Doppler spectrum respectively. Note that the center-zone I_C and the side-zone I_S are actually the intervals selected for array error estimation. They are expressed in (14) and depicted by Figure 2, where B_C is the bandwidth of the center-zone, f_L is the deviation of the frequency at the near edge of side-zone from $f_{\eta c}$, and f_H is the deviation of the frequency at the far edge of side-zone from $f_{\eta c}$.

$$\begin{cases} I_C = \left\{ \tilde{f}_\eta \,\middle|\, \left|\tilde{f}_\eta - f_{\eta c}\right| \le B_C/2 \right\} \\ I_S = \left\{ \tilde{f}_\eta \,\middle|\, f_L \le \left|\tilde{f}_\eta - f_{\eta c}\right| \le f_H \right\} \end{cases} \tag{14}$$

When $\hat{\gamma}$ approaches the true value γ, mainlobe ambiguities can be well suppressed, then J_{MSCR} tends to the minimum value. Hence, we design the MSCR method to obtain an estimate of $\hat{\gamma}$ by minimizing J_{MSCR}:

$$\hat{\gamma} = \arg \min_{\hat{\gamma}} J_{\mathrm{MSCR}} \tag{15}$$

From (11), we have $\sum\limits_{\tilde{f}_\eta} E(|\hat{S}(\tilde{f}_\eta)|^2) = \hat{\gamma}^{\mathbf{H}} \sum\limits_{\tilde{f}_\eta} E(\mathbf{Z}(\tilde{f}_\eta))\hat{\gamma}$. Then, we have

$$J_{\mathrm{MSCR}} = \left(\hat{\gamma}^{\mathbf{H}}\mathbf{R}_S\hat{\gamma}\right)\big/\left(\hat{\gamma}^{\mathbf{H}}\mathbf{R}_C\hat{\gamma}\right) \tag{16}$$

where $\mathbf{R}_C \triangleq \sum\limits_{\tilde{f}_\eta \in I_C} E(\mathbf{Z}(\tilde{f}_\eta))$ and $\mathbf{R}_S \triangleq \sum\limits_{\tilde{f}_\eta \in I_S} E(\mathbf{Z}(\tilde{f}_\eta))$. According to (12), we have

$$E\left(\mathbf{Z}(\tilde{f}_\eta)\right) = \mathbf{W}_q^{\mathbf{H}}(f_\eta)\mathbf{R}_X(f_\eta)\mathbf{W}_q(f_\eta); \quad \tilde{f}_\eta \in I_{Q,q} \tag{17}$$

where $\mathbf{R}_X(f_\eta) = E(\mathbf{X}(f_\eta)\mathbf{X}^{\mathbf{H}}(f_\eta))$ is the covariance matrix of received data. Since $\mathbf{R}_X(f_\eta)$ is positive definite, it's easy to verify that $E(\mathbf{Z}(\tilde{f}_\eta))$ is positive definite. Therefore, $\mathbf{R}_C$ and $\mathbf{R}_S$ are positive definite as well. In practice, $\mathbf{R}_X(f_\eta)$ is obtained as the average over a number of range cells.

Eigen-decomposition of $\mathbf{R}_C$ gives $\mathbf{R}_C = \mathbf{U}\mathbf{\Sigma}\mathbf{U}^{\mathbf{H}}$, where $\mathbf{U} = [\mathbf{u}_1, \mathbf{u}_2, \ldots, \mathbf{u}_M]$ and $\mathbf{\Sigma} = \mathrm{diag}(\boldsymbol{\lambda}_1, \boldsymbol{\lambda}_2, \ldots, \boldsymbol{\lambda}_M)$, where $\boldsymbol{\lambda}_m > 0$ is the eigenvalue associated with the eigenvector $\mathbf{u}_m$. Introducing the notations $\mathbf{D} \triangleq \mathbf{U}\mathbf{\Sigma}_{sqrt}\mathbf{U}^{\mathbf{H}}$ and $\hat{\mathbf{y}} \triangleq \mathbf{D}\hat{\boldsymbol{\gamma}}$, where $\mathbf{\Sigma}_{sqrt} = \mathrm{diag}(\boldsymbol{\lambda}_1^{1/2}, \boldsymbol{\lambda}_2^{1/2}, \ldots, \boldsymbol{\lambda}_M^{1/2})$, we have

$$\hat{\boldsymbol{\gamma}} = \mathbf{D}^{-1}\hat{\mathbf{y}} \tag{18}$$

and (16) reduces to

$$J_{\mathrm{MSCR}} = \left(\hat{\mathbf{y}}^{\mathbf{H}}\mathbf{B}\hat{\mathbf{y}}\right)\Big/\left(\hat{\mathbf{y}}^{\mathbf{H}}\hat{\mathbf{y}}\right) \tag{19}$$

where $\mathbf{B} \triangleq \mathbf{D}^{-1}\mathbf{R}_S\mathbf{D}^{-1}$ and $\mathbf{D}^{-1} = \mathbf{U}\mathbf{\Sigma}_{sqrt}^{-1}\mathbf{U}^{\mathbf{H}}$.

At first, we can obtain $\hat{\mathbf{y}}$ by solving $\hat{\mathbf{y}} = \arg\min_{\hat{\mathbf{y}}} J_{\mathrm{MSCR}}$. According to the Rayleigh-Ritz theorem [15], we have $\hat{\mathbf{y}} = \mathbf{e}_{\min}$, where $\mathbf{e}_{\min}$ is the eigenvector associated with the minimum eigenvalue of matrix $\mathbf{B}$. From (18), then, we have $\hat{\boldsymbol{\gamma}} = \mathbf{D}^{-1}\mathbf{e}_{\min}$. Ultimately, phase error of the mth channel is obtained as

$$\hat{\varphi}_m = \angle\left(\hat{\gamma}_m\hat{\gamma}_1^*\right) \tag{20}$$

where $\angle(\cdot)$ indicates the phase of a complex value and $(\cdot)^*$ indicates conjugate operation.

3.2. Influence of Nonuniform Sampling

AWLS method actually obtains the phase error estimate by minimizing the side-zone power while MSCR method obtains the phase error estimate by minimizing the ratio between side-zone power and center zone power. Mathematically, AWLS method can be expressed by

$$\hat{\boldsymbol{\gamma}} = \arg\min_{\hat{\boldsymbol{\gamma}}} J_{\mathrm{AWLS}} \tag{21}$$

where $J_{\mathrm{AWLS}} \triangleq P_S$. Taking advantage of the SNR information for every Doppler bin [13], AWLS method outperforms OSM and SSCM especially for low SNR. Apparently, both MSCR and AWLS methods are based on the assumption that most of the power is constrained in the center-zone while the side-zone takes up lesser power.

The 'optimal' sampling rate is $\mathrm{PRF}_{opt} = 2v_s/(M \cdot \Delta x)$ [7]. When system PRF deviates from PRF_{opt}, the system suffers from nonuniform sampling. As indicated in [7], nonuniform sampling may lead to strong scaling of the noise, especially for the Doppler subbands far from Doppler centroid. Consequently, reconstructed Doppler spectrum may be contaminated seriously by output noise spectrum. Sidelobe spectral components out of the interval $[f_{\eta c} - \frac{Qf_s}{2}, f_{\eta c} + \frac{Qf_s}{2}]$ will be weighted by the reconstruction network as well and then contribute to azimuth ambiguities of azimuth multichannel SAR. Accordingly, reconstructed spectrum is contaminated by the sidelobe spectrum as well. Therefore, nonuniform sampling may degrade the performance of AWLS and MSCR methods. For a realistic SAR system which is well designed, azimuth ambiguity power is usually far lower then noise power. At this point, the additive noise components are the dominant factors degrading the estimation performance.

4. SIMULATION RESULTS

Single channel data acquired by an X-band airborne SAR system are used to synthesize multi-channel data in the following experiments. Doppler bandwidth B_{amb} is about $400\,\mathrm{Hz}$ while the operated azimuth sampling rate $\mathrm{PRF}_{raw} = 1000\,\mathrm{Hz}$, sensor velocity $v_s = 112\,\mathrm{m/s}$. Size of the raw data block adopted for the experiments is 6048 (azimuth) by 1024 (range). Azimuth aliased data of $M = 4$ channels are obtained by re-sampling the raw data. The first channel is set as the reference channel and is not added with phase error while the other three channels are added with uniformly distributed random phase errors on open interval $(-180°, 180°)$. In addition, complex white Gaussian noise is added to all channels.

Figure 3 illustrates the data re-sampling. In Figure 3(a), the nth azimuth sample of the mth channel is acquired by sampling the $[(2m-1)+8(n-1)]$th azimuth sample of the raw data, resulting in a reduced sampling rate $\text{PRF} = \text{PRF}_{raw}/8 = 125\,\text{Hz}$ and an effective $\Delta x = 0.448\,\text{m}$. After the re-sampling, data size of each channel is 756 (azimuth) by 1024 (range). In Figure 3(b), the nth azimuth sample of the mth channel is acquired by sampling the $[(2m-1)+7(n-1)]$th azimuth sample of the raw data, resulting in a higher $\text{PRF} = \text{PRF}_{raw}/7 = 142.86\,\text{Hz}$. Data size of each channel is then 864 (azimuth) by 1024 (range). As depicted by the figures, the re-sampling scheme shown in Figure 3(a) results in uniform sampling while the re-sampling scheme shown in Figure 3(b) results in nonuniform sampling.

Averaged root-mean-square error (ARMSE) of the phase error estimates given by

$$\text{ARMSE} = \frac{1}{M-1} \sum_{m=2}^{M} \sqrt{\frac{1}{K} \sum_{k=1}^{K} |\hat{\varphi}_{k,m} - \varphi_m|^2} \tag{22}$$

is adopted to evaluate estimation performance, where $\hat{\varphi}_{k,m}$ is the phase error estimate of the mth channel of the kth trial and K the number of trials. In the experiments, 300 trials are implemented. For OSM and SSCM the 400 Doppler bins centered around Doppler centroid are used. According to the values of B_{amb}, M, and PRF, signal subspace dimension and noise subspace dimension are assumed to be *three* and *one*, respectively. For MSCR method, we set $Q = M = 4$, $B_C = B_{amb}/3$, $f_L = B_{amb}/6$, and $f_H = Q \cdot \text{PRF}/2$. For AWLS method, the PDB is set as $B_{amb}/3$ as well.

Experiment results are shown in Figure 4, where Figure 4(a) and Figure 4(b) give the simulated results when PRF are 125 Hz and 142.86 Hz, respectively. As shown in Figure 4(a), when PRF = 125 Hz, AWLS and MSCR methods give similar performance and outperform OSM and SSCM. With
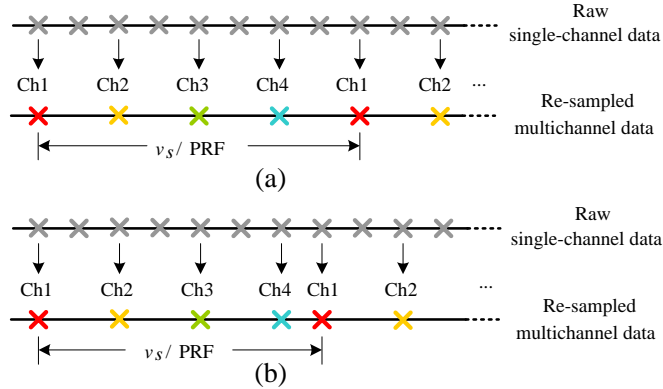
Figure 3. Azimuth positions of the raw single channel data and the synthesized multichannel data. (a) Uniform sampling, PRF = 125 Hz. (b) Nonuniform sampling, PRF = 142.86 Hz.
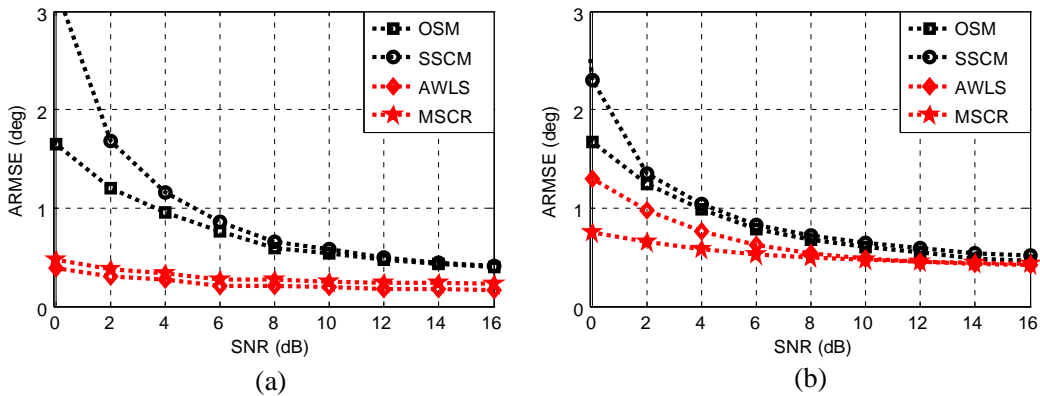
Figure 4. ARMSE of the phase error estimates versus SNR in the cases of (a) uniform sampling, PRF = 125 Hz; (b) nonuniform sampling, PRF = 142.86 Hz.

the increase of PRF, the system suffers from nonuniform sampling, e.g., PRF = 142.86 Hz. As shown in Figure 4(b), strong scaling effect of nonuniform sampling leads to the performance degradation of AWLS and MSCR. However, by making use of the SNR information for every Doppler bin, AWLS and MSCR still perform better than OSM and SSCM. Resulting from the use of the center-zone information, we observe that MSCR method gives the best estimation performance, especially for low SNR.

5. CONCLUSION

MSCR method is presented for array error estimation of azimuth multichannel SAR. Firstly, similar to AWLS method, MSCR method makes use of the SNR information for every Doppler bin. Secondly, it takes advantage of the side-zone and center-zone information simultaneously. Compared with OSM, SSCM, and AWLS method, therefore, MSCR method achieves significantly improved performance on phase error estimation especially for a low SNR. Validity and solidity of the method are confirmed by experiment results.

REFERENCES

1. Chan, Y. K. and V. C. Koo, "An introduction to synthetic aperture radar (SAR)," *Progress In Electromagnetics Research B*, Vol. 2, 27–60, 2008.
2. An, D. X., Z. M. Zhou, X. T. Huang, and T. Jin, "A novel imaging approach for high resolution squinted spotlight SAR based on the deramping-based technique and azimuth NLCS principle," *Progress In Electromagnetics Research*, Vol. 123, 485–508, 2012.
3. Xu, H., J. Gao, and J. Li, "A variable PRF imaging method for high squint diving SAR," *Progress In Electromagnetics Research*, Vol. 135, 215–229, 2013.
4. Chen, J., J. Gao, Y. Zhu, W. Yang, and P. Wang, "A novel image formation algorithm for high-resolution wide-swath spaceborne SAR using compressed sensing on azimuth displacement phase center antenna," *Progress In Electromagnetics Research*, Vol. 125, 527–543, 2012.
5. Huang, Y., P. V. Brennan, D. Patrick, I. Weller, P. Roberts, and K. Hughes, "FMCW based MIMO imaging radar for maritime navigation," *Progress In Electromagnetics Research*, Vol. 115, 327–342, 2011.
6. Currie, A. and M. A. Brown, "Wide-swath SAR," *Proc. Inst. Elect. Eng. — Radar, Sonar, Navigat.*, Vol. 139, No. 2, 122–135, 1992.
7. Krieger, G., N. Gebert, and A. Moreira, "Multidimensional waveform encoding: A new digital beamforming technique for radar remote sensing," *IEEE Trans. Geosci. Remote Sens.*, Vol. 46, No. 1, 31–46, Jan. 2008.
8. Bordoni, F., M. Younis, and G. Krieger, "Ambiguity suppression by azimuth phase coding in multichannel SAR systems," *IEEE Trans. Geosci. Remote Sens.*, Vol. 50, No. 2, 617–629, Feb. 2012.
9. Wang, T. and Z. Bao, "Improving the image quality of spaceborne multiple-aperture SAR under minimization of sidelobe clutter and noise," *IEEE Geosci. Remote Sens. Lett.*, Vol. 3, No. 3, 387–301, Jul. 2006.
10. Gebert, N., "Multi-channel azimuth processing for high-resolution wideswath," Ph.D. Dissertation, IHE, University of Karlsruhe, Karlsruhe, Germany, 2009.
11. Li, Z., Z. Bao, H. Wang, and G. Liao, "Performance improvement for constellation SAR using signal processing techniques," *IEEE Trans. Aerosp. Electron. Syst.*, Vol. 42, No. 2, 436–452, Apr. 2006.
12. Yang, T., Z. Li, Y. Liu, and Z. Bao, "Channel error estimation methods for multichannel SAR systems in azimuth," *IEEE Geosci. Remote Sens. Lett.*, Vol. 10, No. 3, 548–552, May 2013.
13. Liu, Y., Z. Li, T. Yang, and Z. Bao, "An adaptively weighted least square estimation method of channel mismatches in phase for multichannel SAR systems in azimuth," *IEEE Geosci. Remote Sens. Lett.*, Vol. 11, No. 2, 439–443, Feb. 2014.
14. Oppenheim, A. V., R. W. Schafer, and J. R. Buck, *Discrete-time Processing,* Prentice-Hall, Upper Saddle River, New Jersey, 1999.
15. Zhang, X. D., *Matrix Analysis and Applications,* Tsinghua University Press, Beijing, 2004.